

## A RADIO SUPERNOVA REMNANT ASSOCIATED WITH THE YOUNG PULSAR J1119–6127

FRONEFIELD CRAWFORD<sup>1,8</sup>, B. M. GAENSLER<sup>1,6</sup>, V. M. KASPI<sup>1,2,7</sup>,  
 R. N. MANCHESTER<sup>3</sup>, F. CAMILO<sup>4</sup>, A. G. LYNE<sup>5</sup> AND M. J. PIVOVAROFF<sup>1,9</sup>

## ABSTRACT

We report on Australia Telescope Compact Array observations in the direction of the young high magnetic-field pulsar J1119–6127. In the resulting images we identify a non-thermal radio shell of diameter 15', which we classify as a previously uncatalogued young supernova remnant, G292.2–0.5. This supernova remnant is positionally coincident with PSR J1119–6127, and we conclude that the two objects are physically associated. No radio emission is detected from any pulsar wind nebula (PWN) associated with the pulsar; our observed upper limits are consistent with the expectation that high magnetic-field pulsars produce radio nebulae which fade rapidly. This system suggests a possible explanation for the lack of an associated radio pulsar and/or PWN in many supernova remnants.

*Subject headings:* ISM: individual (G292.2–0.5) – pulsars: individual (PSR J1119–6127) – radio continuum:  
 ISM – stars: neutron – supernova remnants

## 1. INTRODUCTION

Important insight into the formation and evolution of pulsars and supernova remnants (SNRs) can be obtained by finding physical associations between the two classes of object. Pulsars are believed to be formed in supernovae which result from the collapse of massive stars, a scenario which implies that young pulsars and SNRs should be associated. However, there are only about a dozen cases in which such a pairing can be seriously claimed (Kaspi 1998). It is still a matter of debate as to why there are so few pulsar / SNR associations. While there is no doubt that selection effects associated with detecting each type of object can at least partly account for the deficit in associations (Gaensler & Johnston 1995), there is mounting evidence that a significant fraction of SNRs may be associated with objects with very different properties from traditional radio pulsars (Gothelf & Vasisht 2000). Establishing an association between a SNR and any sort of compact object addresses this fundamental issue of what is left behind when a star explodes. In the particular case of associations of radio pulsars with SNRs, studies of such systems provide important constraints on pulsar properties such as their initial spin-periods, magnetic fields, radio luminosities, birth-rates and beaming fractions (e.g. Brazier & Johnston 1999).

Meanwhile, the young pulsars usually associated with SNRs lose their rotational kinetic energy at a rapid rate. These pulsars deposit this energy into their surroundings in the form of a magnetized relativistic particle wind. This wind can interact with the ambient medium to produce an observable pulsar wind nebula (PWN), the study of which can provide information on both the pulsar's wind and surrounding environment (e.g. Frail et al. 1996).

1.1. *The young pulsar J1119–6127*

The 408-ms pulsar J1119–6127 (Camilo et al. 2000a) was recently discovered in the Parkes multibeam pulsar survey (Lyne et al. 2000; Camilo et al. 2000b). This pulsar has a very small characteristic age  $\tau_c \equiv P/2\dot{P} = 1.6$  kyr and a very high dipole magnetic field,  $B \approx 3.2 \times 10^{19} (P\dot{P})^{1/2} \text{ G} = 4.1 \times 10^{13} \text{ G}$ , where  $P$  and  $\dot{P}$  are the pulsar's spin-period and period derivative, respectively. Assuming that neither the pulsar's magnetic moment nor moment of inertia are evolving with time, it can be shown that an upper limit on the pulsar's age is  $1.7 \pm 0.1$  kyr (Camilo et al. 2000a). In Table 1 we compare the properties of PSR J1119–6127 to the other five known pulsars for which  $\tau_c < 5$  kyr. It can be seen that each of these other young pulsars is associated with radio emission from a SNR and/or PWN, and it thus seems reasonable to suppose that PSR J1119–6127 might similarly have an associated SNR or PWN.

Indeed, examination of the highest-resolution radio data available for the region (Fig. 1; see also Green et al. 1999) shows emission in the vicinity of the pulsar suggestive of the morphology expected for a SNR. However, artifacts produced by the nearby bright H II regions NGC 3603 and NGC 3576 (see De Pree, Nysewander, & Goss 1999 and references therein), along with further image defects occurring at the boundary between adjacent fields, seriously limit the sensitivity and image quality in this region. We therefore have undertaken more detailed observations of the field surrounding PSR J1119–6127 in an attempt to ascertain the nature of emission in the region, as described in Section 2. In Section 3 we show that the emission seen in the pulsar's vicinity is a non-thermal shell, G292.2–0.5, and set upper limits on the radio emission from a PWN at the pulsar's position. In Section 4 we argue that G292.2–0.5 is a

<sup>1</sup>Department of Physics and Center for Space Research, Massachusetts Institute of Technology, 70 Vassar Street, Cambridge, MA 02139

<sup>2</sup>Department of Physics, Rutherford Physics Building, McGill University, 3600 University Street, Montreal, Quebec, H3A 2T8, Canada

<sup>3</sup>Australia Telescope National Facility, CSIRO, PO Box 76, Epping, NSW 1718, Australia

<sup>4</sup>Columbia Astrophysics Laboratory, Columbia University, 550 W. 120th Street, New York, NY 10027

<sup>5</sup>University of Manchester, Jodrell Bank Observatory, Macclesfield, Cheshire SK11 9DL, United Kingdom

<sup>6</sup>Hubble Fellow

<sup>7</sup>Alfred P. Sloan Research Fellow

<sup>8</sup>Current address: Management and Data Systems Division, Lockheed Martin Corporation, PO Box 8048, Philadelphia, PA 19101

<sup>9</sup>Current address: Therma-Wave Inc., 1250 Reliance Way, Fremont, CA 94539

previously unidentified SNR associated with PSR J1119–6127, while in Section 5 we account for the absence of a radio PWN as being a result of the pulsar’s high magnetic field. The results of X-ray observations of this system are presented in a companion paper by Pivovaroff et al. (2000).

## 2. OBSERVATIONS

We have undertaken radio observations towards PSR J1119–6127 with the Australia Telescope Compact Array (ATCA) (Frater, Brooks, & Whiteoak 1992), an east-west synthesis telescope consisting of six 22-m antennas, located near Narrabri, NSW, Australia. These observations are summarized in Table 2; in each observation data were taken simultaneously at 1.4 and 2.5 GHz. The bandwidth at each observing frequency was 128 MHz, split into 32 4-MHz channels. Observations were carried out in pulsar-gating mode, in which complex correlations from the antenna pairs were recorded 32 times per pulse period, and then folded at this period before being written to disk. All four Stokes parameters were recorded for each spectral channel and pulse bin. All observations used the same pointing center, located  $\sim 1'$  from the position of the pulsar. An absolute flux density scale was determined by observations of PKS B1934–638, assuming flux densities for this source of 14.9 and 11.1 Jy at 1.4 and 2.5 GHz respectively (Reynolds 1994). Both the time-dependent gain and the polarization leakage parameters of each antenna were determined via regular observations of PKS B1036–697. The final combined data set consisted of 1172860 complex correlations spread over 60 baselines ranging between 31 m and 5878 m.

## 3. ANALYSIS AND RESULTS

### 3.1. Total intensity images

Data were calibrated in the MIRIAD package, using standard approaches unless otherwise stated (Sault & Killeen 1999). Data were first edited to eliminate portions corrupted by interference; flux density, antenna gain and polarization calibrations were then applied. Images of total intensity were then formed at both 1.4 and 2.5 GHz, using data from all pulse bins, and employing a uniform weighting scheme to minimize side lobes. To enhance the surface brightness sensitivity, images were formed using only baselines at projected spacings shorter than  $7.5 \text{ k}\lambda$ . Furthermore, at 2.5 GHz we also discarded data at spacings shorter than  $0.5 \text{ k}\lambda$ , to reduce the effect of confusing side-lobes produced by the two bright nearby H II regions. The images were then deconvolved using a maximum entropy routine (Cornwell & Evans 1985; Narayan & Nityananda 1986), and the resulting images convolved with a Gaussian restoring beam of dimensions  $29'' \times 25''$  (at 1.4 GHz) and  $21'' \times 20''$  (at 2.5 GHz), corresponding to the diffraction-limited resolutions of the respective data sets.

The resulting images are shown in Figures 2 and 3. The rms sensitivity in each image is  $\sim 0.5 \text{ mJy beam}^{-1}$ , which is ten and five times worse than the theoretical sensitivity expected at 1.4 GHz and 2.5 GHz, respectively. This is not surprising given the very complicated nature of the region and the presence of bright H II regions in the vicinity.

In the 1.4-GHz image in Figure 2, it is clear that the extended emission seen in the lower-resolution MGPS data shown in Figure 1 is now resolved into a distinct limb-brightened elliptical shell of dimensions  $14' \times 16'$ . After applying a correction for

a non-zero background, we estimate a 1.4-GHz flux density for this shell of  $5.6 \pm 0.3 \text{ Jy}$ . Based on its Galactic coordinates, we designate this shell G292.2–0.5.

This shell can also be seen at 2.5 GHz in Figure 3; however the image quality at this frequency is poorer than at 1.4 GHz, because the confusing H II regions are further into the wings of the primary beam than at 1.4 GHz, and their side lobes are consequently more difficult to deconvolve. At 2.5 GHz the measured flux density of G292.2–0.5 is  $1.6 \pm 0.1 \text{ Jy}$ . This value is a significant underestimate on the source’s true flux density, because at this higher frequency the largest scale to which the interferometer is sensitive is  $\sim 7'$ , implying that much of the emission from this source is not detected in our observations.

In Figure 4 we show an *IRAS* 60- $\mu\text{m}$  image of the region (Cao et al. 1997). While there is significant infrared emission associated with the bright H II regions to the west of the pulsar, there is no detectable emission coincident with G292.2–0.5. The weak infrared source IRAS J11169–6111 can be seen close to the position of PSR J1119–6127; this source is probably not associated with the pulsar (see discussion by Pivovaroff et al. 2000).

We determined an accurate position for the pulsar as follows. First, a delay was applied to each frequency channel corresponding to a dispersion measure of  $713 \text{ pc cm}^{-3}$ .<sup>10</sup> The data corresponding to off-pulse bins were then subtracted from on-pulse data in the  $u - v$  plane, and the position of the pulsar determined by fitting the Fourier transform of a point source to the resulting data set. The resulting position and associated uncertainty for PSR J1119–6127 are RA (J2000)  $11^{\text{h}}19^{\text{m}}14.30 \pm 0.02$ , Dec. (J2000)  $-61^{\circ}27'49.5 \pm 0.2''$ . This position, marked in all the images with a cross, puts the pulsar coincident with the geometric center of the SNR, within the uncertainties of such a determination.

### 3.2. Spectral index determination

A measurement of the spectral index,  $\alpha$ , for G292.2–0.5 (where  $S_\nu \propto \nu^\alpha$ ) is essential for determining whether this source is a SNR or not. However, a spectral index cannot be determined directly from the 1.4 and 2.5 GHz images shown in Figures 2 and 3, because the  $u - v$  coverage of the two images differs considerably. We thus spatially filtered the two images as follows (see also Gaensler et al. 1999). We first corrected the 1.4 GHz image for primary beam attenuation, and then applied the attenuation corresponding to the shape of the primary beam at 2.5 GHz. We then Fourier transformed the resulting image, and re-sampled it using the transfer function of the 2.5 GHz observations. The resulting data set then had properties identical to the 2.5 GHz data, except that the intensity distribution on the sky was that at 1.4 GHz. This data set was then imaged and deconvolved in the same way as for the 2.5 GHz data. Both this resulting image and the original 2.5 GHz image in Figure 3 were then smoothed to a final resolution of  $30''$ .

These two images could then be directly compared to determine the spectral index of the emission. To make this determination, we applied the approach of “spectral tomography” (Katz-Stone & Rudnick 1997) to G292.2–0.5. This involved scaling the 2.5 GHz image by a trial spectral index  $\alpha_t$ , and then subtracting this scaled image from the 1.4 GHz image, to form a difference image  $I_{\alpha_t}$ , defined by:

<sup>10</sup>This was the best estimate available at the time, and differs slightly from the published dispersion measure of  $707 \pm 2 \text{ pc cm}^{-3}$  (Camilo et al. 2000a); this small difference does not affect the results.

$$I_{\alpha_t} = I_{1.4} - \left( \frac{1.4}{2.5} \right)^{\alpha_t} I_{2.5}, \quad (1)$$

where  $I_{1.4}$  and  $I_{2.5}$  are the images to be compared at 1.4 and 2.5 GHz respectively. The spectral index,  $\alpha$ , of a particular feature is simply the value of  $\alpha_t$  at which its emission blends into the background. An uncertainty in this spectral index is estimated by finding the range in values of  $\alpha_t$  at which the residual at this position in the difference image becomes significant.

In Figure 5 we show a series of such difference images for the region surrounding the bright south-eastern rim of G292.2–0.5, for trial spectral indices in the range  $0.0 > \alpha_t > -1.1$  at intervals  $\Delta \alpha_t = 0.1$ . For a trial spectral index  $\alpha_t = 0$ , the significant negative residuals indicate that the emission from the shell has a non-thermal ( $\alpha < 0$ ) spectrum. By finding the trial spectral index at which the residuals make the transition from negative to positive, we estimate that the spectral index of this part of G292.2–0.5 is  $\alpha = -0.6 \pm 0.2$ . Other parts of the shell are significantly fainter at 2.5 GHz, and a spectral index determination is correspondingly more difficult. However, results for these regions also suggest a spectral index  $\alpha \sim -0.6$ .

### 3.3. Polarization

SNRs are significantly linearly polarized, typically at a fractional level of 10–20%. Thus the presence or absence of linear polarization is a further useful discriminant as to whether a source is a SNR. Unfortunately there is a significant off-axis response in linear polarization, meaning that instrumental artifacts due to the bright H II regions NGC 3603 and NGC 3576 dominate emission in Stokes  $Q$  and  $U$  at the position of G292.2–0.5. We were thus unable to make any measurement of the polarization properties of this object.

### 3.4. Limits on emission from a radio PWN

There is no obvious emission at the pulsar's position in either of Figures 2 or 3 which might be associated with a PWN. In order to put quantitative limits on the surface brightness of such a source, we carried out the following steps.

First, we excluded pulse bins corresponding to times when the pulsar was “on”, emission from which could potentially mask emission from a coincident PWN (Gaensler et al. 1998; Stappers, Gaensler, & Johnston 1999). Next, we subtracted a model of the emission from the shell itself and from external sources from the  $u-v$  data. The resulting image had greatly improved sensitivity to emission at or near the pulsar's position (see Gaensler, Bock, & Stappers 2000). We then carried out a series of trials, stepping through all angular sizes between the resolution of the data and the extent of G292.2–0.5. For each trial, we simulated a PWN by adding to the  $u-v$  data the Fourier transform of a faint circular disk centered on the pulsar, and with diameter equal to the trial angular size. We then made an image of the region, convolving it with a Gaussian of FWHM slightly smaller than the size of the disk to give maximal sensitivity to structures on that scale. We repeated this process at increasing flux densities for the simulated PWN, until it could be detected in the resulting image at the  $5\sigma$  level (e.g. Green & Scheuer 1992; Gaensler, Bock, & Stappers 2000). The surface brightness of this marginally detectable disk was taken as our sensitivity to a PWN at a given angular size.

Figure 6 shows a plot of the corresponding 1.4 and 2.5 GHz upper limits on surface brightness of any PWN, as a function of

angular size. In both cases, we have scaled our results to an observing frequency of 1 GHz by assuming a PWN spectral index  $\alpha = -0.3$  as seen for the Crab Nebula.

### 4. AN ASSOCIATION BETWEEN G292.2–0.5 AND PSR J1119–6127?

In order for a source to be classified as a shell-type SNR, it needs to have a limb-brightened morphology, show a non-thermal spectral index ( $\alpha \sim -0.5$ ), have a high radio to infrared flux ratio, and be linearly polarized. We have shown that G292.2–0.5 meets all of the first three criteria (as explained in Section 3, polarization measurements were not possible for this source due to instrumental effects). We therefore conclude that G292.2–0.5 is a previously unidentified SNR.

The 1-GHz surface brightness of this SNR<sup>11</sup> is  $\Sigma \sim 4.7 \times 10^{-21} \text{ W m}^{-2} \text{ Hz}^{-1} \text{ sr}^{-1}$ . This value is not particularly faint, being of order the approximate completeness limit of the entire sample of Galactic SNRs (Gaensler & Johnston 1995). Thus the fact that this SNR had until now gone undetected is not a result of lack of sensitivity, but is entirely due to the severe selection effects associated with identifying SNRs in complicated regions. Undoubtedly there remain many other reasonably bright SNRs which are similarly hidden beneath the side-lobes from adjacent strong sources.

Associations between pulsars and SNRs are usually judged on agreement in distance, agreement in age, the space velocity inferred from the offset of the pulsar with respect to the SNR's apparent center, and the likelihood of a chance coincidence between the two sources. We now consider each of these criteria in turn.

As discussed by Camilo et al. (2000a), the distance inferred for PSR J1119–6127 from its dispersion measure is  $>30$  kpc, and is certainly a severe overestimate. Meanwhile, no distance estimate is possible for SNR G292.2–0.5 from the available data. Thus we are unable to determine whether distances to the two sources are comparable. Camilo et al. (2000a) note that the Carina spiral arm of the Galaxy crosses the line of sight at distances of 2.4 and 8 kpc, and therefore assume that the pulsar's true distance falls somewhere in this range. We make a similar assumption for SNR G292.2–0.5, and in future discussion denote the distance to the source as  $5d_5$  kpc. The radius of the SNR is then  $R = (10.9 \pm 0.7)d_5$  pc.

We can derive an approximate age for SNR G292.2–0.5 as follows. For a uniform ambient medium of pure hydrogen with density  $n_0 \text{ cm}^{-3}$ , the mass swept up by the SNR is  $\sim 140n_0d_5^3 M_\odot$ . For typical ejected masses and ambient densities, the SNR is then partly in transition to the adiabatic (Sedov-Taylor) phase of expansion (see e.g. Dohm-Palmer & Jones 1996). We can therefore use the expected rate of expansion in the adiabatic phase to derive an upper limit on the SNR age of  $(7 \pm 1)(n_0/E_{51})^{1/2}d_5^{5/2}$  kyr, where  $E_{51}$  is the kinetic energy of the explosion in units of  $10^{51}$  erg. For a typical value  $n_0/E_{51} = 0.2$  (Frail, Goss, & Whiteoak 1994), we find that the age of the SNR must be less than  $\sim 3d_5^{5/2}$  kyr. This is in good agreement with the upper limit on the pulsar's age of  $1.7 \pm 0.1$  kyr estimated by Camilo et al. (2000a) from pulsar timing.

We estimate that the pulsar is offset by no more than  $\sim 1'$  from the geometric center of the SNR. If this geometric center corresponds to the site of the supernova explosion, and if the

<sup>11</sup>using the usual definition  $\Sigma_\nu \equiv S_\nu/\theta^2$ , where  $\theta$  is the angular diameter of the SNR, and where the effects of limb-brightening have been disregarded

pulsar and SNR are physically associated, then a typical transverse velocity for the pulsar of  $500V_{500}$  km s $^{-1}$  implies an upper limit on the age for the system of  $< 2.9d_5/V_{500}$  kyr, consistent with the ages estimated separately for the pulsar and the SNR.

As discussed above, G292.2–0.5 has a surface brightness comparable to the completeness limit of the Galactic SNR population. Thus a good estimate of the probability of a chance alignment between the pulsar and the SNR can be made by considering the distribution of known SNRs down to this surface brightness limit. In a representative region of the Galactic Plane covering the range  $270^\circ \leq l \leq 330^\circ$ ,  $|b| \leq 2^\circ$ , there are 20 other SNRs brighter than G292.2–0.5 (Whiteoak & Green 1996; Green 2000). The probability that such a SNR should have its center lying by chance within 1' of PSR J1119–6127 is therefore  $\sim 7 \times 10^{-5}$ . Even if the geometric center of a SNR does not correspond to its true center, the offset between the two is probably no more than  $\sim 25\%$  of the SNR's radius (e.g. Dohm-Palmer & Jones 1996; Zaninetti 2000), so that the probability of a chance alignment is still  $\ll 10^{-3}$ .

To summarize, we find that SNR G292.2–0.5 is of comparable age to PSR J1119–6127, that the offset of the pulsar from the SNR's center is consistent with the youth of the system, and that the probability is low that the two sources align so closely by chance. We therefore conclude that it is highly likely that PSR J1119–6127 and SNR G292.2–0.5 are physically associated.

## 5. IMPLICATIONS OF THE NON-DETECTION OF A RADIO PWN

### 5.1. PWNe around young pulsars

The Crab pulsar is by far the best-studied young pulsar. In the evolutionary picture inferred for this pulsar and its associated nebula, a young pulsar is born spinning rapidly ( $P \lesssim 20$  ms). Over the next thousand years, the pulsar undergoes only modest spin-down so that it is still spinning rapidly and has a high spin-down luminosity. The interaction of the resulting pulsar wind with the ambient medium produces a radio-bright PWN. The other two rapidly spinning pulsars in Table 1, PSRs B0540–69 and J0537–6910, also have these properties.

However, the other three young pulsars in Table 1, namely PSRs J1846–0258, B1509–58 and J1119–6127, are all of a comparable age to the Crab-like pulsars, but spin much more slowly ( $P > 100$  ms) and have much higher magnetic fields ( $B > 10^{13}$  G). If, like the Crab-like pulsars, these high-field pulsars were born spinning rapidly, then we can infer that they lost most of their rotational energy early in their lives. Given this important difference in their evolutionary histories, it is perhaps not reasonable to expect that they should power radio-bright PWNe like those produced by the Crab-like pulsars. While PSR J1846–0258 is associated with a radio PWN (Becker & Helfand 1984; Gotthelf et al. 2000), no radio PWN has been detected around PSR B1509–58 (Gaensler et al. 1999), although the sensitivity to such a source is limited by the complicated nature of the region. Furthermore, we have shown here that to even more stringent limits, no PWN is present around PSR J1119–6127 either.

In Table 3 we list the properties of a representative group of radio PWN. We plot the resulting sizes and 1-GHz surface brightnesses of these sources in Figure 6, all scaled to a common distance of 5 kpc. Two types of PWN are shown: those with a “static” morphology, in which the PWN is confined by the gas pressure of the surrounding medium (e.g. Arons 1983;

Reynolds & Chevalier 1984, hereafter RC84), and those with a “bow-shock” morphology, where the PWN is confined by ram pressure resulting from the pulsar's motion with respect to its environment (e.g. Frail et al. 1996). It can be seen from the upper limits derived in Section 3 and also plotted in Figure 6 that each of the PWNe considered would have been easily detected in our observations.

In the case of PSR B1509–58, we plot the upper limit of Gaensler et al. (1999). The angular size for this PWN has been estimated by assuming that the PWN has freely expanded since the pulsar's birth with an expansion velocity  $V = 1700$  km s $^{-1}$  as measured for the Crab Nebula (Trimble 1968). It can be seen that the upper limits on the brightness of a PWN around PSR J1119–6127 are ten times more stringent than those for PSR B1509–58, and thus are potentially a better test of the evolution of high-magnetic field pulsars.

### 5.2. A simple model for PWN evolution

An explanation for the absence of a radio PWN around PSR B1509–58 was proposed by Bhattacharya (1990), who pointed out that even if a high magnetic-field pulsar is born spinning rapidly, it will quickly slow down to a long period due to severe magnetic braking. At later times, there is therefore no significant energy injection into the PWN from the pulsar, and the energetics of the nebula are dominated by the significant losses which it experiences due to expansion into the ambient medium. The net result is that a PWN associated with a high-field pulsar should have an observable lifetime which is very brief, corresponding to the reduced period for which the pulsar provides significant amounts of energy to the nebula.

The radio luminosity evolution of a PWN has been considered in detail by several authors (e.g. Pacini & Salvati 1973; RC84). In these studies, it is found that the evolution of a radio PWN can be divided into two main stages. The transition occurs at a time  $t \approx \tau_0 \equiv P_0/(n-1)\dot{P}_0$ , where  $P_0$  and  $\dot{P}_0$  are the initial period and period derivative of the pulsar, respectively, and  $n$  is the pulsar's braking index (assumed to not vary with time).

In the first stage of evolution ( $t \lesssim \tau_0$ ), the pulsar is a significant source of energy for the expanding PWN. For times immediately preceding  $t = \tau_0$ , the radio luminosity of the PWN at a given frequency decreases with time as  $L_\nu(t) \propto t^{(7\alpha-3)/4}$  (RC84), where  $\alpha$  is the radio spectral index of the PWN defined by  $S_\nu \propto \nu^\alpha$ . The radio luminosity decreases, despite the fact that the pulsar continues to inject energy into the PWN, because of losses resulting from expansion of the nebula.

In the succeeding stage of evolution ( $t \gtrsim \tau_0$ ), the pulsar has now transferred the bulk of its initial rotational energy into the PWN, and no longer injects significant amounts of energy into it. The radio luminosity of the PWN now decreases more steeply than in the first stage, so that  $L_\nu \propto t^{-2\gamma}$ , where  $\gamma = 1-2\alpha$  is the energy-index of the injected particle spectrum.

RC84 consider two cases for the evolution of a PWN: case “NE”, in which the energies in relativistic electrons and magnetic fields evolve independently, and case “E”, in which there is equipartition between particles and magnetic fields.

Analytic solutions for the evolution of the PWN are only possible for case NE. In this case, we find that at a frequency  $\nu$ , and at a time  $t > \tau_0$ ,<sup>12</sup> the spectral luminosity of the nebula is given by (RCW84):

$$L_\nu = K L_0^{(7-\gamma)/8} \tau_0^{(1+9\gamma)/8} (p-\gamma)^{-1} t^{-2\gamma} \quad (2)$$

<sup>12</sup>which is the only time-range of interest for the pulsars being considered here

where  $L_0 \equiv 4\pi^2 I \dot{P}_0 / P_0^3$  is the initial spin-down luminosity of the pulsar,  $p = (n+1)/(n-1)$  and  $K$  is a constant of proportionality.  $K$  depends on the mass of the slowly-moving ejecta and on the details of the injected particle spectrum (RC84) — we assume that these quantities are the same for each of the pulsars we are considering.

The ratio of spectral luminosities  $L_{\nu,1}$  and  $L_{\nu,2}$  for two PWNe with ages  $t_1$  and  $t_2$  respectively, and with similar spectral indices, is then:

$$\frac{L_{\nu,1}}{L_{\nu,2}} = \left( \frac{L_1}{L_2} \right)^{(7-\gamma)/8} \left( \frac{\tau_1}{\tau_2} \right)^{(1+9\gamma)/8} \left( \frac{p_1 - \gamma}{p_2 - \gamma} \right)^{-1} \left( \frac{t_1}{t_2} \right)^{-2\gamma}, \quad (3)$$

where  $L_{1,2}$ ,  $\tau_{1,2}$  and  $p_{1,2}$  are the initial spin-down luminosities  $L_0$ , the “initial characteristic ages”  $\tau_0$  and the parameter  $p = (n+1)/(n-1)$  for the two pulsars, respectively.

Since the initial surface magnetic field has the dependency  $B_0 \propto (P_0 \dot{P}_0)^{1/2}$ , we can write  $\tau_0 \equiv P_0 / (n-1) \dot{P}_0 \propto P_0^2 / (n-1) B_0^2$ . Similarly, we find that  $L_0 \propto \dot{P}_0 / P_0^3 \propto P_0^2 / B_0^4$ , so that:

$$\frac{L_{\nu,1}}{L_{\nu,2}} = \left( \frac{P_1}{P_2} \right)^{\frac{-13+11\gamma}{4}} \left( \frac{B_1}{B_2} \right)^{\frac{3-5\gamma}{2}} \left( \frac{n_1-1}{n_2-1} \right)^{-\frac{1+9\gamma}{8}} \left( \frac{p_1 - \gamma}{p_2 - \gamma} \right)^{-1} \left( \frac{t_1}{t_2} \right)^{-2\gamma}, \quad (4)$$

where  $P_{1,2}$ ,  $B_{1,2}$  and  $n_{1,2}$  are the initial periods, initial magnetic fields and braking indices of the two pulsars.

We now convert spectral luminosities into 1-GHz surface brightnesses using the fact that  $\Sigma \propto L / (Vt)^2$ , where we have assumed that the PWN is freely expanding. Assuming that  $\alpha = -0.3$  as for the Crab Nebula, we have that  $\gamma = 1 - 2\alpha = 1.6$ , so that:

$$\frac{\Sigma_1}{\Sigma_2} = \left( \frac{P_1}{P_2} \right)^{+1.15} \left( \frac{B_1}{B_2} \right)^{-2.50} \left( \frac{n_1-1}{n_2-1} \right)^{-1.93} \left( \frac{p_1 - \gamma}{p_2 - \gamma} \right)^{-1} \left( \frac{V_1}{V_2} \right)^{-2.0} \left( \frac{t_1}{t_2} \right)^{-5.2}. \quad (5)$$

By making the assumptions that  $P_0$  and  $V$  for PSR J1119–6127 and its associated PWN are similar to the corresponding values for the Crab, that the characteristic age of PSR J1119–6127 is a good approximation to its true age, and that the pulsar’s surface magnetic field does not significantly evolve with time, we can then use Equation (5) to predict the brightness of a radio PWN associated with PSR J1119–6127 for case NE. Using the parameters listed in Table 4, we predict a 1 GHz surface brightness for a radio PWN of  $\Sigma \simeq 6 \times 10^{-22} \text{ W m}^{-2} \text{ Hz}^{-1} \text{ sr}^{-1}$ . It can be seen from Figure 6 that this predicted value is significantly fainter than the surface brightness of any detected radio PWN, and is consistent with the upper limits derived in Section 3.

No analytic solution is possible for case E. However, Figure 2 of RC84 shows that the main difference between cases NE and E is that the radius of the expanding PWN is  $\sim 2$  times smaller in the latter case. The predicted surface brightness (plotted in Figure 6) is then  $\sim 4$  times larger than for case NE, but it still below the observed upper limits.

Note that while the direct dependency of radio luminosity on initial period in Equation (5) is weak, a longer initial period would also imply that the pulsar’s true age was smaller than its characteristic age — the strong dependence of  $\Sigma$  on  $t$  must then also be taken into account. For example, Camilo et al. (2000a) show that for an initial period  $P_0 = 200$  ms, the true

age for PSR J1119–6127 would only be 1.2 kyr. In this case, the parameters in Table 4 would then cause us to underestimate the surface brightness by a factor  $\sim 100$ , and would result in a predicted surface brightness well above our sensitivity limits. Our model thus argues in favor of a small initial period for PSR J1119–6127.

We can also apply this model to PSR B1509–58, for which we predict a 1-GHz surface brightness  $\Sigma \sim 8 \times 10^{-21} \text{ W m}^{-2} \text{ Hz}^{-1} \text{ sr}^{-1}$ , in agreement with the upper limit set by Gaensler et al. (1999). For the apparently younger PSR J1846–0258, Equation (5) predicts  $\Sigma \sim 7 \times 10^{-20} \text{ W m}^{-2} \text{ Hz}^{-1} \text{ sr}^{-1}$ . While this is approximately a factor of 2 fainter than the observed surface brightness of the associated PWN, this source has a significantly different spectral index than the Crab Nebula ( $\alpha = 0$ ; Becker & Helfand 1984), and so it is not reasonable to apply a simple scaling from the properties of the Crab as has been done here. Furthermore, while braking indices have been measured for PSRs B1509–58 and J1119–6127 (Kaspi et al. 1994; Camilo et al. 2000a), no such measurement has yet been made for PSR J1846–0258, and its characteristic age may thus not be a good approximation to its true age.

## 6. CONCLUSIONS

Radio observations of the young pulsar J1119–6127 have revealed a limb-brightened radio shell, G292.2–0.5, of diameter  $\sim 15'$ . The spectral index  $\alpha = -0.6 \pm 0.2$  measured for this shell, together with its lack of infrared emission, argue that G292.2–0.5 is a previously unidentified SNR. The small age inferred for G292.2–0.5, together with the proximity of its geometric center to the position of PSR J1119–6127, argue for a physical association between the two objects.

Radio emission from a pulsar-powered nebula was not detected in our observations. We have shown that our observed upper limits are consistent with the expectation that the pulsar spun down rapidly to long periods and dumped the bulk of its energy into the nebula at early times. The energy losses from subsequent expansion of the nebula have caused the radio emission to rapidly fade so that it is now well below the detection threshold of our observations.

The presence of a pulsar within a SNR is usually inferred either directly, via detection of pulsations, or indirectly, through identification of a pulsar wind nebula within the SNR. The fact that both PSRs B1509–58 and J1119–6127 are faint radio pulsars with no detectable radio PWNe suggests that many other young SNRs which have only been studied at radio wavelengths could similarly contain pulsars which are too faint to detect (or which are beaming away from us), and which do not power detectable radio PWNe. The failure to detect radio pulsars and/or PWNe in many SNRs could thus possibly be explained if pulsars with high magnetic fields comprise a significant fraction of the pulsar population. In X-rays, young pulsars generally have higher luminosities, broader beams and more prominent nebulae than in the radio, so that imaging these systems at higher energies might be a better way to infer their presence.

We thank the referee, Steve Reynolds, for his many useful corrections and suggestions, and for his patient explanations of the results from RC84. The Australia Telescope is funded by the Commonwealth of Australia for operation as a National Facility managed by CSIRO. B.M.G. acknowledges the support of NASA through Hubble Fellowship grant HST-HF-01107.01-A awarded by the Space Telescope Science Institute, which

is operated by the Association of Universities for Research in Astronomy, Inc., for NASA under contract NAS 5–26555. F. Crawford and V.M.K. were partly supported by a National Science Foundation Career Award (AST-9875897). F. Camilo ac-

knowledges the support of NASA grant NAG 5-3229. This research has made use of NASA's Astrophysics Data System Abstract Service and of the SIMBAD database, operated at CDS, Strasbourg, France.

## REFERENCES

Arons, J. 1983, *Nature*, 302, 301.

Becker, R. H. & Helfand, D. J. 1984, *ApJ*, 283, 154.

Bhattacharya, D. 1990, *J. Astrophys. Astr.*, 11, 125.

Brazier, K. T. S. & Johnston, S. 1999, *MNRAS*, 305, 671.

Camilo, F., Kaspi, V. M., Lyne, A. G., Manchester, R. N., Bell, J. F., D'Amico, N., McKay, N. P. F., & Crawford, F. 2000a, *ApJ*, 541, 367.

Camilo, F. et al. 2000b, in *Pulsar Astronomy — 2000 and Beyond*, IAU Colloquium 177, ed. M. Kramer, N. Wex, & R. Wielebinski, (San Francisco: Astronomical Society of the Pacific), 3.

Cao, Y., Terebey, S., Prince, T. A., & Beichman, C. A. 1997, *ApJS*, 111, 387.

Cornwell, T. J. & Evans, K. F. 1985, *A&A*, 143, 77.

De Pree, C. G., Nysewander, M. C., & Goss, W. M. 1999, *AJ*, 117, 2902.

Dohm-Palmer, R. C. & Jones, T. W. 1996, *ApJ*, 471, 279.

Frail, D. A., Giacani, E. B., Goss, W. M., & Dubner, G. 1996, *ApJ*, 464, L165.

Frail, D. A., Goss, W. M., & Whiteoak, J. B. Z. 1994, *ApJ*, 437, 781.

Frater, R. H., Brooks, J. W., & Whiteoak, J. B. 1992, *J. Electr. Electron. Eng. Aust.*, 12, 103.

Gaensler, B. M., Bock, D. C.-J., & Stappers, B. W. 2000, *ApJ*, 537, L35.

Gaensler, B. M., Brazier, K. T. S., Manchester, R. N., Johnston, S., & Green, A. J. 1999, *MNRAS*, 305, 724.

Gaensler, B. M. & Johnston, S. 1995, *MNRAS*, 277, 1243.

Gaensler, B. M., Stappers, B. W., Frail, D. A., & Johnston, S. 1998, *ApJ*, 499, L69.

Gotthelf, E. V. & Vasisht, G. 2000, in *Pulsar Astronomy — 2000 and Beyond*, IAU Colloquium 177, ed. M. Kramer, N. Wex, & R. Wielebinski, (San Francisco: Astronomical Society of the Pacific), 699.

Gotthelf, E. V., Vasisht, G., Boylan-Kolchin, M., & Torii, K. 2000, *ApJ*, 542, L37.

Green, A. J., Cram, L. E., Large, M. I., & Ye, T. 1999, *ApJS*, 122, 207. (<http://www.astrop.physics.usyd.edu.au/MGPS/>).

Green, D. A. 2000, *A Catalogue of Galactic Supernova Remnants* (2000 August Version), (Cambridge: Mullard Radio Astronomy Observatory). (<http://www.mrao.cam.ac.uk/surveys/snrs/>).

Green, D. A. & Scheuer, P. A. G. 1992, *MNRAS*, 258, 833.

Kaspi, V. M. 1998, in *Neutron Stars and Pulsars: Thirty Years after the Discovery*, ed. N. Shibasaki, N. Kawai, S. Shibata, & T. Kifune, (Tokyo: Universal Academy Press), p. 401.

Kaspi, V. M., Manchester, R. N., Siegman, B., Johnston, S., & Lyne, A. G. 1994, *ApJ*, 422, L83.

Katz-Stone, D. M. & Rudnick, L. 1997, *ApJ*, 488, 146.

Lyne, A. G. et al. 2000, *MNRAS*, 312, 698.

Marshall, F. E., Gotthelf, E. V., Zhang, W., Middleditch, J., & Wang, Q. D. 1998, *ApJ*, 499, L179.

Narayan, R. & Nityananda, R. 1986, *Ann. Rev. Astr. Ap.*, 24, 127.

Pacini, F. & Salvati, M. 1973, *ApJ*, 186, 249.

Pivovaroff, M., Kaspi, V. M., Camilo, F., Gaensler, B. M., & Crawford, F. 2000, *ApJ*, submitted.

Reynolds, J. E. 1994, *ATNF Technical Document Series*, 39.3040. ([http://www.narrabri.atnf.csiro.au/observing/users\\_guide/html/node215.html](http://www.narrabri.atnf.csiro.au/observing/users_guide/html/node215.html)).

Reynolds, S. P. & Chevalier, R. A. 1984, *ApJ*, 278, 630 (RC84).

Sault, J. R., J. & Killeen, N. E. B. 1999, *The Miriad User's Guide*, (Sydney: Australia Telescope National Facility). (<http://www.atnf.csiro.au/computing/software/miriad>).

Seward, F. D., Harnden, F. R., & Helfand, D. J. 1984, *ApJ*, 287, L19.

Seward, F. D. & Harnden Jr., F. R. 1982, *ApJ*, 256, L45.

Staelin, D. H. & Reifenstein, III, E. C. 1968, *Science*, 162, 1481.

Stappers, B. W., Gaensler, B. M., & Johnston, S. 1999, *MNRAS*, 308, 609.

Trimble, V. 1968, *AJ*, 73, 535.

Whiteoak, J. B. Z. & Green, A. J. 1996, *A&AS*, 118, 329. (<http://www.physics.usyd.edu.au/astrop/wg96cat/>).

Zaninetti, L. 2000, *A&A*, 356, 1023.

TABLE 1  
PULSARS WITH  $\tau_c < 5$  KYR

Pulsar	$P^a$ (ms)	$\tau_c^b$ (kyr)	$B^c$ ( $10^{12}$ G)	$\dot{E}^d$ ( $10^{36}$ erg s $^{-1}$ )	Associated SNR/PWN	Radio SNR?	Radio PWN?	Reference
J1846–0258 <sup>e</sup>	324	0.7	48	8	G29.7–0.3 (Kes 75)	Y	Y	Gotthelf et al. (2000)
B0531+21	33	1.3	3.8	450	G184.6–5.8 (Crab Nebula)	N	Y	Staelin & Reifenstein (1968)
B1509–58	150	1.6	15	18	G320.4–1.2 (MSH 15–52)	Y	N	Seward & Harnden (1982)
<b>J1119–6127</b>	<b>408</b>	<b>1.6</b>	<b>41</b>	<b>2</b>	<b>G292.2–0.5</b>	<b>Y</b>	<b>N</b>	<b>Camilo et al. (2000a); this paper</b>
B0540–69	50	1.7	5.0	150	G279.7–31.5 (0540–69.3)	Y	Y	Seward, Harnden & Helfand (1984)
J0537–6910 <sup>e</sup>	16	5.0	0.9	480	G279.6–31.7 (N 157B)	N	Y	Marshall et al. (1998)

NOTE.—Entries ranked by characteristic age.

<sup>a</sup>Period of rotation.

<sup>b</sup>Characteristic age,  $\tau_c \equiv P/2\dot{P}$ .

<sup>c</sup>Inferred surface dipolar magnetic field,  $B \approx 3.2 \times 10^{19} (P\dot{P})^{1/2}$  G.

<sup>d</sup>Spin-down luminosity,  $\dot{E} \approx 4\pi^2 \times 10^{45} \dot{P}/P^3$  erg s $^{-1}$ .

<sup>e</sup>X-ray pulsar only.

TABLE 2  
ATCA OBSERVATIONS OF PSR J1119–6127

Observing Dates	Observing Frequencies (MHz)	Array Configuration	Time on Source (h)
1998 Oct 30-31	1384/2496	6D	9
1998 Nov 1	1344/2240	6D	5
1999 Nov 25-26	1384/2496	0.375	9
1999 Dec 14	1384/2496	1.5A	9

TABLE 3  
SIZES AND SURFACE BRIGHTNESSES OF SELECTED RADIO PULSAR WIND NEBULAE

PWN or Associated SNR	Other Name	$d^a$ (kpc)	$\theta^b$ (arcmin)	$S_{1\text{ GHz}}^c$ (Jy)	$\log \Sigma^d$ (W m $^{-2}$ Hz $^{-1}$ sr $^{-1}$ )
G184.6–5.8	Crab Nebula, SN 1054	2.5	6	1040	-17.4
G279.7–31.5	0540–69.3	50	0.08	0.09	-17.7
G21.5–0.9		5.5	1.2	6	-18.2
G5.4–1.2 <sup>e</sup>		5	0.07	0.01	-18.5
G279.6–31.7	N 157B	50	1.5	2.75	-18.7
G29.7–0.3	Kes 75	19	0.5	0.3	-18.8
G328.4+0.2	MSH 15–57	17	5	16	-19.0
G130.7+3.1	3C 58	3	8	33	-19.1
G34.7–0.4 <sup>e</sup>	W 44	3	1	0.3	-19.4
G326.3–1.8	MSH 15–56	4	7	14	-19.4
G74.9+1.2	CTB 87	12	7	9	-19.6
G320.4–1.2 <sup>f</sup>	MSH 15–52	5	4	...	<-19.6
G292.2–0.5 <sup>f</sup>		~5	4	...	-22.0

NOTE.—Data from Green (2000) and references therein.

<sup>a</sup>Distance to PWN.

<sup>b</sup>Mean angular diameter of PWN.

<sup>c</sup>1-GHz flux density of PWN.

<sup>d</sup>1-GHz surface brightness of PWN.

<sup>e</sup>Bow-shock nebula.

<sup>f</sup>Radio PWN not detected. Angular size is derived using expansion velocity of Crab Nebula ( $V \sim 1700$  km/s) and characteristic age of associated pulsar. For G320.4–1.2, upper limit on surface brightness is that obtained by Gaensler et al. (1999); for G292.2–0.5, surface brightness is that predicted by the model described in the text.

TABLE 4  
INPUT PARAMETERS TO PWN MODEL

Parameter	PSR B0531+21 / Crab Nebula	PSR J1119–6127
Initial pulsar spin period, $P_0$ (ms)	16	16 (assumed)
Initial surface magnetic field, $B_0$ (G)	$3.8 \times 10^{12}$	$4.1 \times 10^{13}$
Pulsar age, $t$ (kyr)	1.0	1.7
Pulsar braking index, $n$	2.51	2.91
PWN expansion velocity, $V$ (km s $^{-1}$ )	1700	1700 (assumed)

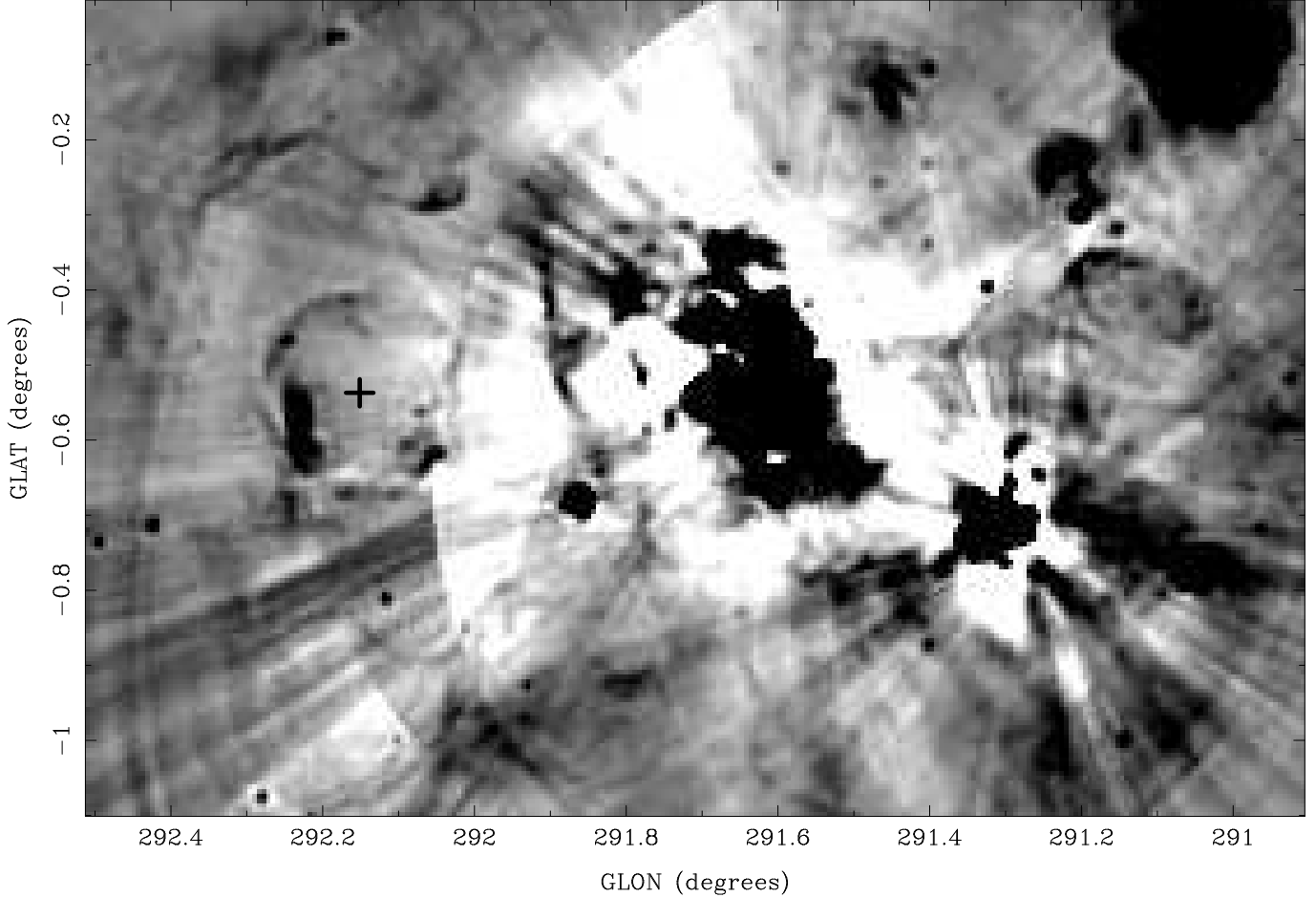


FIG. 1.— An image of the region surrounding PSR J1119–6127 taken from the Molonglo Galactic Plane Survey (MGPS; Green et al. 1999), at a frequency of 843 MHz and an angular resolution of  $\sim 1'$ . Here and in subsequent images, the position of PSR J1119–6127, as determined from pulsar-gating, is indicated by a cross. The bright H II regions NGC 3603 (G291.58–0.41) and NGC 3576 (G291.28–0.71) can be seen to the west of the pulsar.

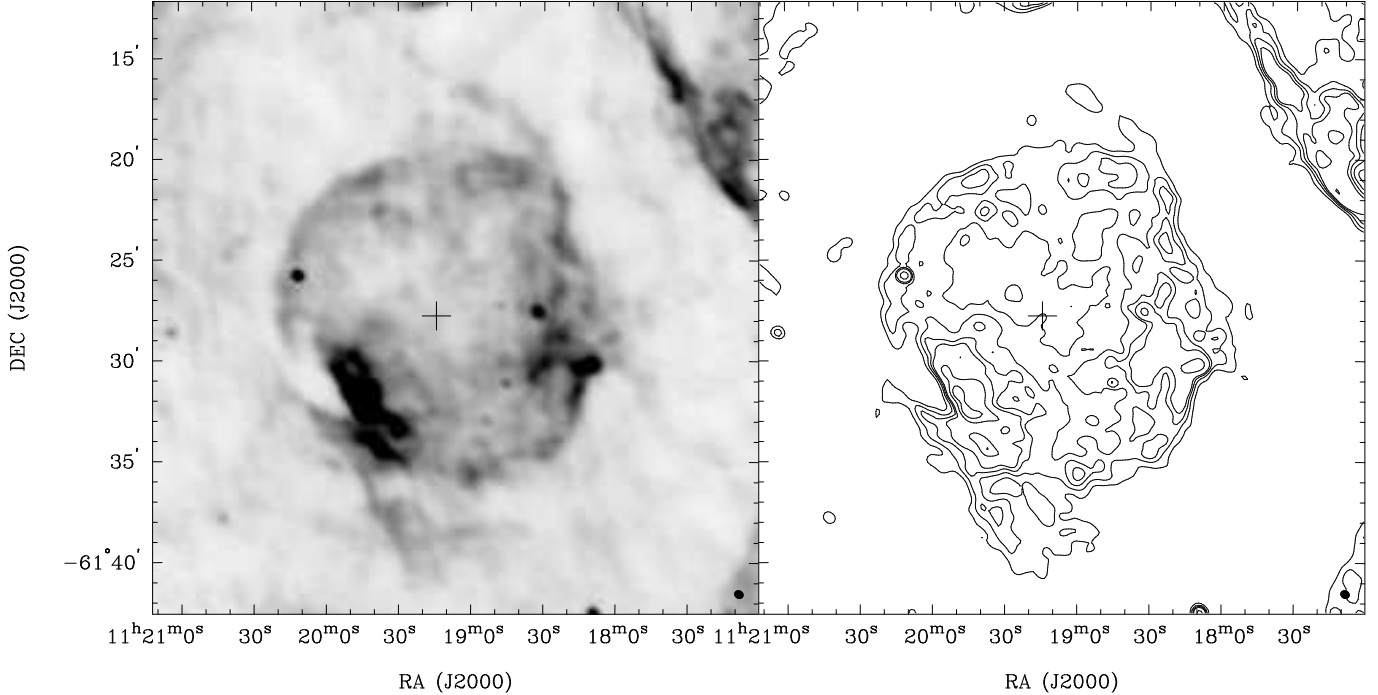


FIG. 2.— ATCA observations of PSR J1119–6127 at 1.4 GHz, using only data corresponding to baselines shorter than 7.5 k $\lambda$ . The greyscale ranges from  $-2$  to  $+18$  mJy beam $^{-1}$ , while contours are shown at levels of 2.5, 5, 7.5, 10, 20 and 30 mJy beam $^{-1}$ . The resolution of the image is  $29'' \times 25''$  (shown at lower right of each panel) and the rms noise level is  $\sim 0.5$  mJy beam $^{-1}$ .

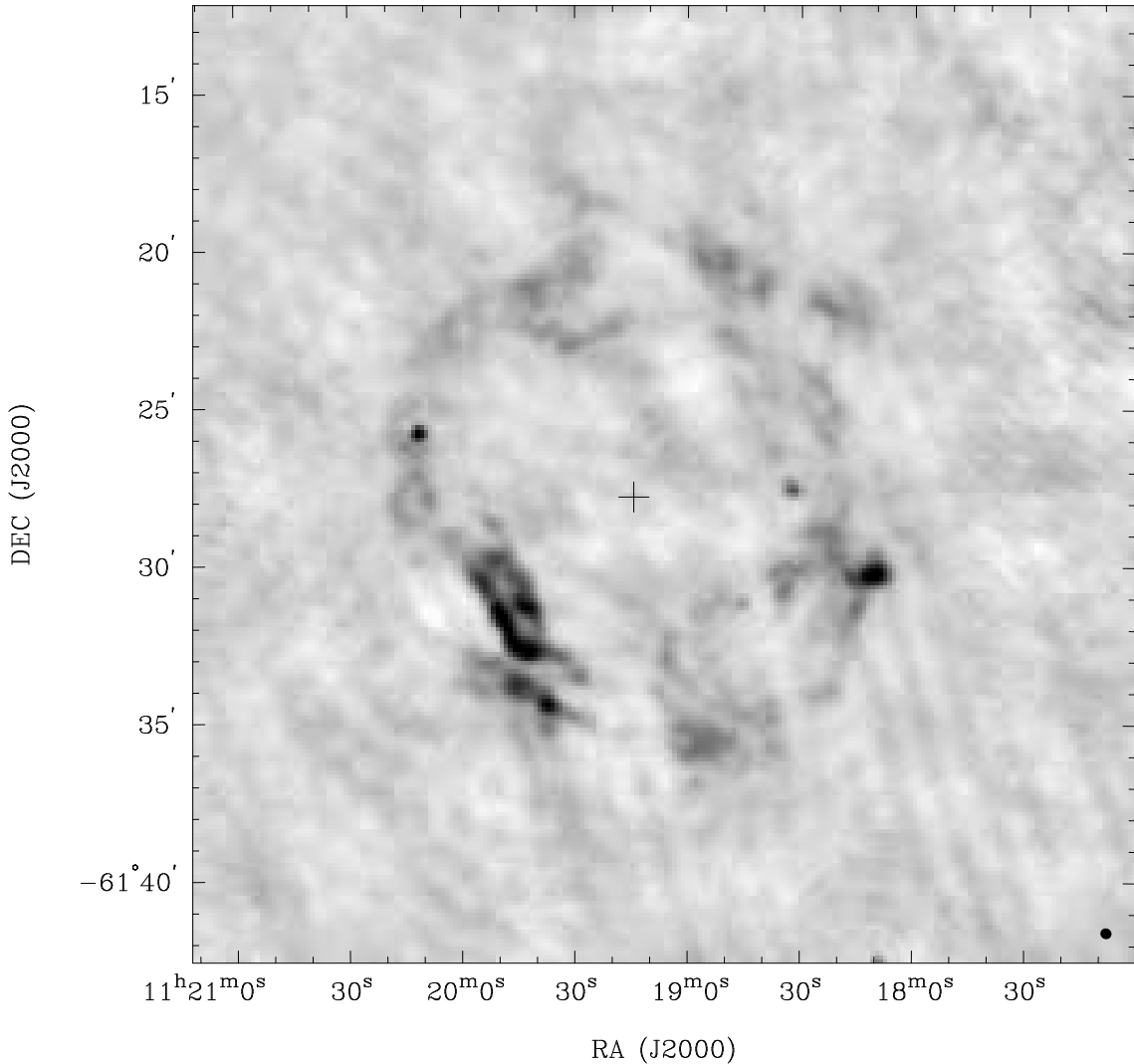


FIG. 3.— ATCA observations of PSR J1119–6127 at 2.5 GHz, using data corresponding to baselines between 0.5 and 7.5  $k\lambda$ . The greyscale ranges from  $-2$  to  $+10$  mJy beam $^{-1}$ , while the resolution is  $21'' \times 20''$ . The image quality is significantly degraded by side-lobes from nearby bright sources.

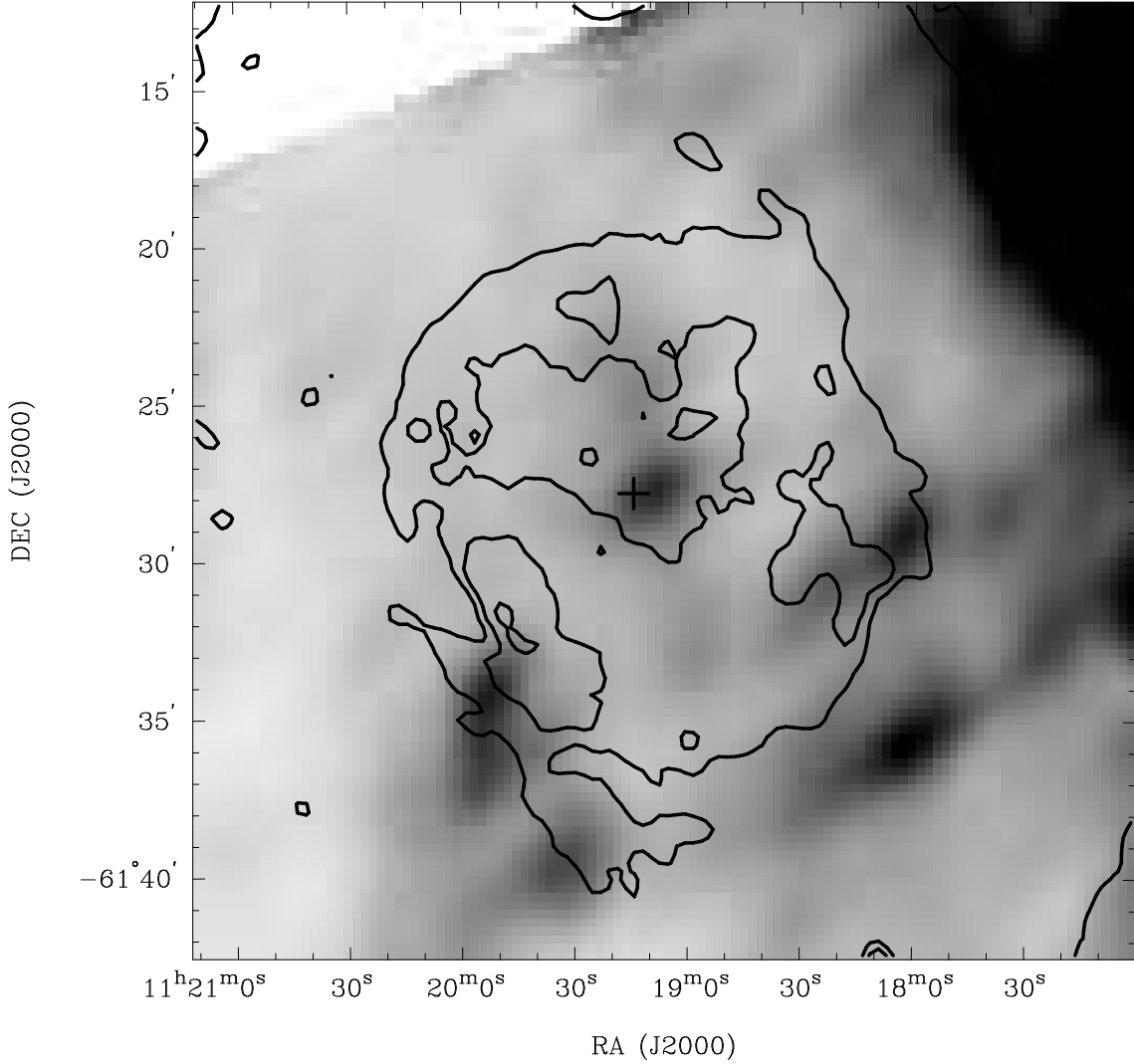


FIG. 4.— Comparison of infrared and radio emission from G292.2–0.5. The greyscale shows the *IRAS* 60- $\mu$ m emission from the region, taken from the *IRAS* Galaxy Atlas (Cao et al. 1997), and ranging between 70 and 400 MJy sr $^{-1}$ . Contours show 1.4 GHz radio emission as in Figure 2, at levels of 3, 10 and 30 mJy beam $^{-1}$ . The infrared source  $\sim 1'$  to the west of PSR J1119–6127 is IRAS J11169–6111.

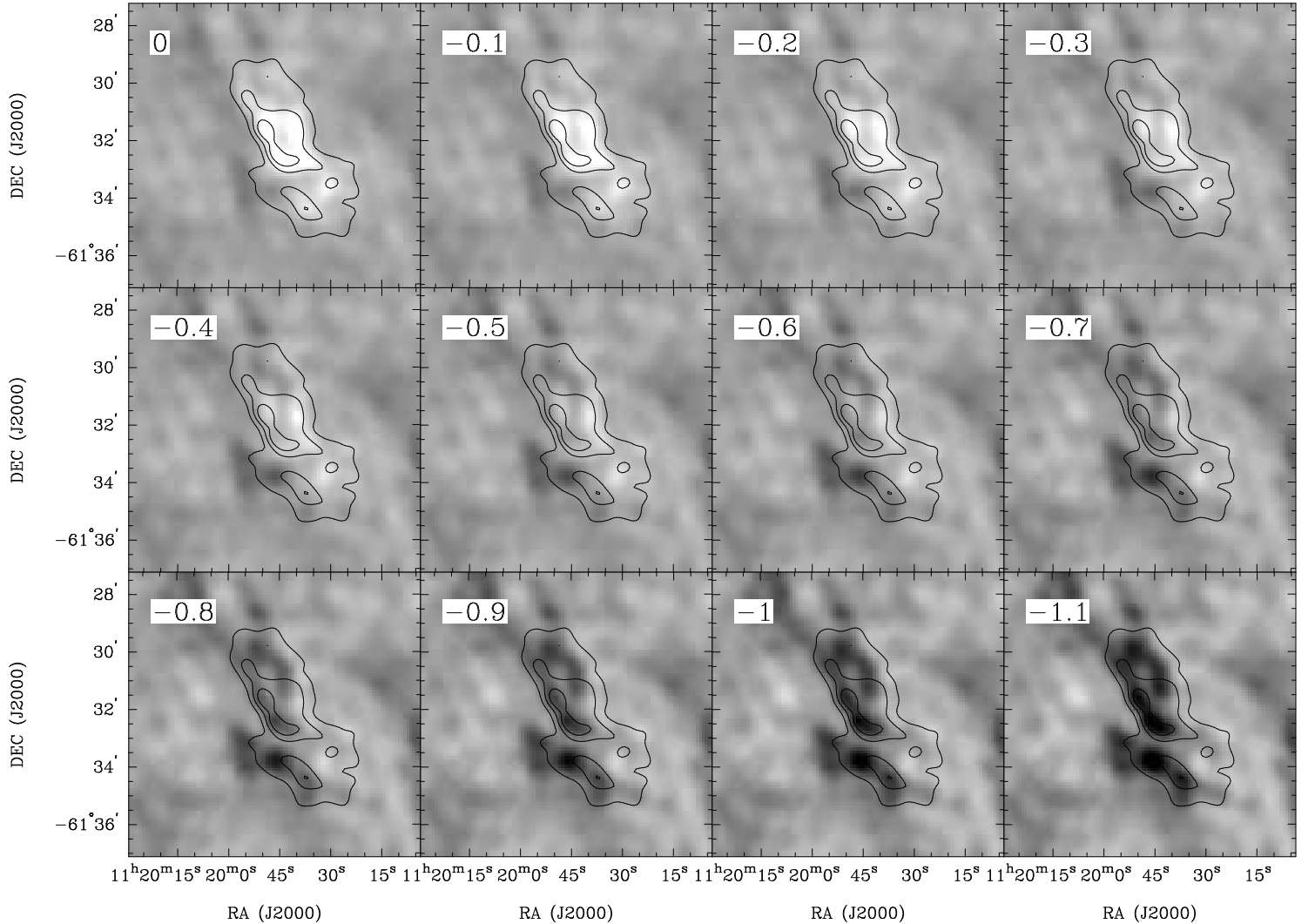


FIG. 5.—Tomographic spectral index images for the bright south-eastern rim of the shell G292.2-0.5. The greyscale shows a series of difference images between 1.4 and 2.5 GHz data which have been matched in  $u-v$  coverage. For each panel, the trial spectral index is shown at upper left. The contours in each panel correspond to the 1.4 GHz data shown in Figure 2, at levels of 10, 20 and 30 mJy beam $^{-1}$ . Light (dark) regions of the image indicate that a feature has a more negative (positive) spectral index than the trial value. The transition from light to dark occurs at a spectral index  $\sim -0.6$ .

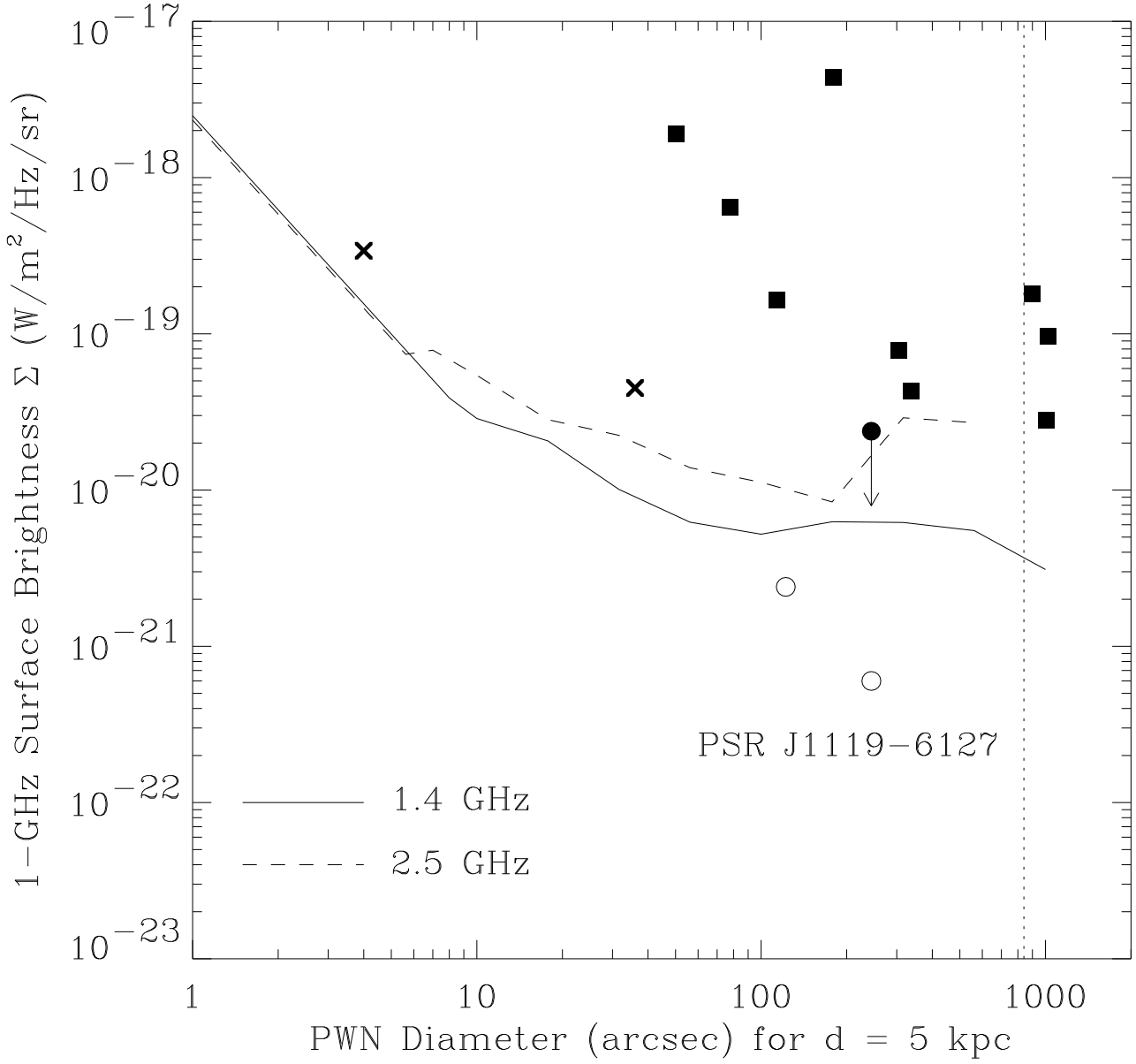


FIG. 6.— 1 GHz surface brightness vs diameter for known radio PWNe, and corresponding upper limits for a PWN associated with PSR J1119–6127. Plotted points correspond to the properties of PWNe as listed in Table 3, scaled to a distance of 5 kpc. Squares indicate static nebulae, crosses indicate nebulae with a bow-shock morphology, while the solid circle indicates the upper limit on a radio PWN associated with PSR B1509–58. The open circles indicate the predicted size and surface brightness for a PWN associated with PSR J1119–6127 using cases NE (lower right) and case E (upper left) of the PWN model of RC84 (see text for details); the solid and dashed lines respectively correspond to the 1.4 and 2.5 GHz observed upper limits on such emission. The vertical dotted line indicates the diameter of G292.2–0.5; this is a hard upper limit on the extent of any PWN associated with PSR J1119–6127.